A quasi-3D viscous-inviscid interaction code: Q3UIC

Ramos García, Néstor; Sørensen, Jens Nørkær; Shen, Wen Zhong

Published in:
Journal of Physics: Conference Series (Online)

Link to article, DOI:
10.1088/1742-6596/555/1/012041

Publication date:
2014

Document Version
Publisher's PDF, also known as Version of record

A quasi-3D viscous-inviscid interaction code: Q^3UIC

2014 J. Phys.: Conf. Ser. 555 012041

(http://iopscience.iop.org/1742-6596/555/1/012041)

A quasi-3D viscous-inviscid interaction code: Q^3UIC

N. R. García, J. N. Sørensen, and W. Z. Shen

Department of Wind Energy, Fluid Mechanics Section, Building 403, Technical University of Denmark, DK-2800 Lyngby Denmark

E-mail: nerga@dtu.dk

Abstract. A computational model for predicting the aerodynamic behavior of wind turbine airfoils under rotation and subjected to steady and unsteady motions developed in [1] is presented herein. The model is based on a viscous-inviscid interaction technique using strong coupling between the viscous and inviscid parts. The rotational effects generated by centrifugal and Coriolis forces are introduced in Q^3UIC via the streamwise and spanwise integral boundary layer momentum equations. A special inviscid version of the code has been developed to cope with massive separation. To check the ability of the code wind turbine airfoils in steady and unsteady conditions for a large range of angles of attack are considered here. Further, the new quasi-3D code Q^3UIC is used to perform a parametric study of a wind turbine airfoil under rotation confined to its boundary layer.

Nomenclature

α	Angle of attack
α_m	Pitching oscillation mean angle of attack
β_w	Angle in between the external and limiting streamlines
δ	Boundary layer thickness
δ_1^*	Streamwise displacement thickness
δ_2^*	Spanwise displacement thickness
Γ	Parabolic vortex total strength
λ	Thwaites' parameter
μ	Fluid dynamic viscosity
ν	Fluid kinematic viscosity
Ω	Rotor angular velocity
$\partial x/\partial y$	Partial derivative of x with respect to y
ρ	Fluid density
σ	Constant source strength
τ_θ	Azimuthal shear stress
τ_r	Radial shear stress
θ_1	Streamwise momentum thickness
θ_2, δ_3	Momentum thickness parameters due to crossflow

$\underline{U}_\infty$	Freestream undisturbed velocity
$\underline{U}_R$	Velocity field created by the vorticity distribution
$\underline{U}_{wake}$	Velocity field created by the inviscid wake
$\underline{U}_{wT}$	Velocity field created by the viscous boundary layer
A	Pitching oscillation amplitude
a, b	Thwaites' moment equation coefficients
B_1	Turbulent Cf relation coefficient
c	Airfoil chord
C_D	Dissipation coefficient
C_d	Drag force coefficient
C_f	Friction coefficient
C_l	Lift force coefficient
C_p	Surface pressure distribution coefficient
dt	Time derivative
e^n	Laminar to turbulent transition method
f_A	Airfoil pitching frequency
H	Shape parameter
H^*	Kinetic energy shape parameter
k_A	Airfoil pitching reduced frequency, $k_A = (\pi f_A c)/U_\infty$
n	Amplification factor
n_c	Critical amplification factor
Q_w	Wind speed
r, θ, z	Cylindrical coordinates
R_O	Rotational number, $\Omega r/U_{rel}$
Re	Reynolds number
$Re_{\theta_1}^{CR}$	Critical Reynolds number based on θ_1
Re_{θ_1}	Reynolds number based on θ_1
s	Streamwise direction
st	Distance between leading edge and transition point
t	Time
TI	Turbulence intensity
u'_e	Potential edge velocity at a unit freestream
u, v, w	Fluid flow velocities
u_e	Boundary layer edge velocity
U_{rel}	Airfoil relative velocity
w_T	Transpiration velocity

1. Introduction

Computers are becoming more powerful with the years, but it is still beyond the limit to perform an optimum design of blades using a Navier-Stokes solver, because of the computing intensive iterative design work between geometry and aerodynamic forces. Historically, it is possible to predict the overall forces on a rotor blade by adding up the aerodynamic forces of each section of the blade using strip theory, such as the way used in the the blade-element theory to compute thrust and power. Nowadays aerodynamic force coefficients used as input to blade-element models (BEM) are obtained from two dimensional airfoil data based on experiments. Occasionally three dimensional corrections are used, usually based in curve fitting.

An alternative method to computing heavy Navier-Stokes solutions, is to use viscous-inviscid interaction methods. In this type of methods a viscous approach is used to compute the boundary layer, while in the outer part the flow is modeled to be purely inviscid. During the last century a lot of effort was put into the development of this technique [2, 3, 4, 5]. During the present work a viscous-inviscid interactive code has been developed where the inviscid part is solved using a potential panel method and the viscous effects are taken into account solving the integral form of the Quasi3D boundary layer r and θ momentum equations with the kinetic energy shape parameter equation in its two dimensional form. A higher order treatment is introduced for the variation of pressure across the boundary layer as a post processing correction.

In the present model a strong coupling between the viscous and inviscid parts is used to cope with separation, overcoming Goldstein's singularity. The code is capable of predicting laminar to turbulent transition either using a numerical trip wire (fixed transition) or a modified e^n transition model (free transition).

A special inviscid version of the code has been developed to cope with massive separation using a double wake model approach. In this model a first wake leaves the trailing edge of the airfoil and a second wake is shed from the separation point downstream. This special model demands knowledge of the position of the separation. However, with a known position of the separation point, the computed pressure distributions are in excellent agreement with experimental results.

Rotational effects are introduced in the model through the integral boundary layer momentum equations in the streamwise and spanwise directions through centrifugal and Coriolis forces. A parametric study on rotational effects in the boundary layer shows that the effect of rotation is to decrease the growth of the boundary layer, delay the onset of separation, and increase the lift coefficient at the same time as the drag is slightly decreased.

2. Numerical method and governing equations

In this section, we describe the governing equations employed in the quasi-3D unsteady viscous-inviscid interactive code. The inviscid part of the flow is solved using a panel method following Hess approach [6], whereas the viscous part is modeled by using the integral boundary layer equations, in laminar or turbulent form, depending on the flow characteristics. The coupling between both parts is done via the already known concept of transpiration velocity [7].

Thwaites' method is used to solve the viscous flow problem from the stagnation point to the downstream station where laminar-turbulent transition takes place. The turbulent flow is modeled with the integral form of the r and θ momentum equations in combination with the kinetic energy shape parameter integral equation and a set of semi-empirical relations. Transition can be forced by the user or predicted by the e^n method with Mack's modification to take into account the free stream turbulent intensity [8].

2.1. Inviscid part

For the two-dimensional incompressible and irrotational flow past an airfoil, the solution can be considered to be a superposition of different elementary solutions using Green's identity, represented by a set of singularities on the airfoil surface contour [9].

To satisfy the Neumann condition on the airfoil surface, a distribution of panels with constant source distribution, $\underline{\sigma}$, is introduced. The Kutta condition is imposed as a constraint on the potential flow solution in which the velocities at the two control points on the lower and upper surface of the panels forming the trailing edge are forced to attain the same magnitude. In order to fulfill the Kutta condition, a rotating onset flow is introduced. In practice this can be accomplished by adding a parabolic vorticity distribution, γ, around the airfoil with zero strength at the upper and lower trailing edge elements.

In unsteady cases, a vortex is shed at each time-step from the airfoil trailing edge with a strength equal to the change of circulation on the airfoil contour, satisfying Kelvin's theorem. The direction of the vortex emission is parallel to either the suction or pressure side of the airfoil.

The effect of the viscous shear layer is simulated via an injection function, known as a transpiration velocity, w_T. More precisely, a source distribution is introduced to generate the transpiration velocity which replaces the non-penetration Neumann condition and creates the strong coupling between the viscous and inviscid parts of the system.

By adding the different fundamental solutions, the resulting velocity distribution around the airfoil can be written as:

$$\underline{U}_{I_p} = \underline{U}_\infty + \Gamma \underline{U}_R + \underline{U}_{wake} + \underline{U}_{wT} \tag{1}$$

where $\underline{U}_\infty$ is the freestream undisturbed velocity field, $\underline{U}_R$ is the velocity field created by the vorticity distribution, $\underline{U}_{wake}$ is the contribution of the inviscid wake and $\underline{U}_{wT}$ adds the velocity field created by the viscous boundary layer.

2.2. Viscous part

In order to perform an integral boundary layer analysis for a rotating airfoil, the full three-dimensional boundary layer equations have to be simplified. The influence of curvature is neglected. Thus, the shape of the actual airfoil section is included in the pressure gradient from the potential flow solution, but not in the boundary layer closure equations.

In differential form, the three-dimensional unsteady incompressible boundary layer equations in cylindrical coordinates of a steady rotating frame of reference can be written as [10]

Continuity

$$\frac{1}{r}\frac{\partial u}{\partial \theta} + \frac{1}{r}\frac{\partial (rv)}{\partial r} + \frac{\partial w}{\partial z} = 0 \tag{2}$$

$\theta-$Momentum

$$\frac{\partial u}{\partial t} + \frac{u}{r}\frac{\partial u}{\partial \theta} + w\frac{\partial u}{\partial z} + v\frac{\partial u}{\partial r} - \frac{u}{r}(2\Omega r - u) = -\frac{1}{\rho r}\frac{\partial p}{\partial \theta} + \frac{1}{\rho}\frac{\partial \tau_\theta}{\partial z} \tag{3}$$

$r-$Momentum

$$\frac{\partial v}{\partial t} + \frac{1}{r}\frac{\partial (uv)}{\partial \theta} + \frac{\partial v^2}{\partial r} + \frac{\partial (vw)}{\partial z} + \frac{v^2}{r} - \frac{u}{r}(u - 2\Omega r) = -\frac{1}{\rho}\frac{\partial p}{\partial r} + \Omega^2 r + \frac{1}{\rho}\frac{\partial \tau_r}{\partial z} \tag{4}$$

To reduce the 3D differential boundary layer equations to the quasi-3D form, a strip theory approach is used in which it is assumed that the flow locally is two-dimensional, following a similar reasoning to Fogarty and Sear [11]. The edge velocity, u_e, can be found using a two dimensional solution of the flow assuming potential flow at the edge of the boundary layer,

$$u_e(s, r) = U_{rel} u'_e(s) \tag{5}$$

$$U_{rel} = \sqrt{(\Omega r)^2 + Q_w^2} \tag{6}$$

where u'_e is the potential velocity at a unit free-stream velocity, (s, r) are the streamwise and spanwise coordinates respectively and U_{rel} is the total relative velocity seen by the airfoil section. Assuming that u'_e is independent of r, the quantity $\frac{\partial u_e}{\partial r}$ can be written as

$$\frac{\partial u_e}{\partial r} = \frac{\partial U_{rel}}{\partial r} u'_e = \frac{2\left(\Omega^2 r\right)}{2\sqrt{(\Omega r)^2 + Q_w^2}} u'_e = \frac{\Omega^2 r}{U_{rel}} u'_e = u_e R_O^2 \frac{1}{r} \tag{7}$$

where R_O is the rotation number defined as the ratio between the rotational speed and the relative velocity,

$$R_O = \frac{\Omega r}{U_{rel}} \tag{8}$$

After integration of the differential equations from the airfoil surface to the edge of the boundary layer for a flat plate and adapting for an airfoil geometry, the r and θ quasi-3D integral momentum boundary layer equations can be written in terms of the boundary layer edge velocity, u_e, and the integral boundary layer parameters $\theta_1, \theta_2, \delta_1^*, \delta_2^*, \delta, \delta_3, C_f$ and β_w as [1]:

$$\frac{\partial \theta_1}{\partial s} = -\frac{1}{u_e^2}\frac{d}{dt}\left(u_e \delta_1^*\right) - \frac{\partial \theta_1}{u_e}\frac{\partial u_e}{\partial s}\left(2 + H\right) + \frac{C_f}{2} + s_w p_r \frac{2R_O l}{u_e c}\delta_2^* \tag{9}$$

$$\frac{\partial \theta_2}{\partial s} = -\frac{2\theta_2}{u_e}\frac{\partial u_e}{\partial s} + tan\beta_w \frac{C_f}{2} - \frac{1}{u_e}\frac{\partial u_e}{\partial r}\left(2\delta_3 + \delta\right) + \frac{l}{c}\left(\theta_1 + \delta_1^* - \delta - \delta_3 + s_w p_r \frac{2R_O}{u_e}\left(\delta - \delta_1^*\right)\right) \tag{10}$$

Turbulent boundary layer closure equations In order to solve the spanwise and streamwise momentum equations (9) and (10), a set of closure relations is used to calculate the integral boundary layer parameters introduced above. For deriving these relations, a crossflow velocity profile v is used which tends to zero as approaching the boundary layer edge, Equation (11). While the streamwise velocity profile is adopted, u, is a power law type, which approaches the freestream velocity at the edge of the boundary layer, Equation (12).

$$\frac{v}{u_e} = tan\left(\beta_W\right)\left(1 - \frac{z}{\delta}\right)^2 \tag{11}$$

$$\frac{u}{u_e} = \left(\frac{z}{\delta}\right)^{\frac{H-1}{2}} \tag{12}$$

Following Lakshminarayana and Govindan [12], the closure equations for the spanwise quantities of a turbulent boundary layer are obtained by integrating the velocity profiles introduced above and can be written as follows

$$\frac{\delta_2^*}{\delta} = -\frac{16H\tan\beta_w}{(H-1)(H+3)(H+5)}\frac{\theta_1}{\delta} \tag{13}$$

$$\frac{\theta_2}{\delta} = -\frac{2tan\beta_w}{(H-1)(H+2)}\frac{\theta_1}{\delta} \tag{14}$$

$$\frac{\delta_3}{\delta} = -\frac{24\left(\tan\beta_w\right)^2}{(H-1)(H+2)(H+3)(H+1)}\frac{\theta_1}{\delta} \tag{15}$$

in terms of streamwise quantities, following Du and Selig [13], the closures applied for δ_1^* and θ_1 are,

$$\frac{\delta_1^*}{\delta} = \frac{H-1}{H+1} \tag{16}$$

$$\frac{\theta_1}{\delta} = \frac{2}{H+1} - \frac{1}{H} \tag{17}$$

The skin-friction closure equation for flows with pressure gradients and rotation effects is based on empirical data for turbulent boundary layers in a rotating channel, as described by [12],

$$C_f = 0.172 Re_{\theta_1}^{-0.268} 10^{-0.678H} \left(1 + B_1 \sqrt{tan\left(\beta_w\right)\left(s - s_t\right)/c}\right) \tag{18}$$

where B_1 is a constant with value 0.52.

In order to take into account the variation of the shape factor parameter, H, the kinetic energy-shape parameter equation is chosen in its two-dimensional unsteady form. The following equation is derived by combining the standard integral streamwise momentum equation and the kinetic energy thickness equation with addition of the unsteady boundary layer quantity terms, [14].

$$\frac{1}{u_e^3}\frac{d}{dt}\left(u_e^2\theta_1\right) + \frac{1}{u_e}\frac{d}{dt}\left(\delta_1^*\right) - \frac{H^*}{u_e^2}\frac{d}{dt}\left(u_e\delta_1^*\right) + \theta_1\frac{dH^*}{ds} + \left[H^*\left(1-H\right)\right]\frac{\theta_1}{u_e}\frac{du_e}{ds} = 2C_D - H^*\frac{C_f}{2} \tag{19}$$

Following Drela's work [4] a set of two-dimensional relations is used to compute the integral boundary layer quantities appearing in Equation (19).

Laminar Thwaites' method [15] solves the streamwise momentum integral equation in terms of a parameter λ which is more stable and faster for computing attached laminar boundary layers than the complete integral momentum equations which requires of a set of closure relations to be solved.

$$\theta_1^2 = b\nu u_e \int_0^x u_e^{-a-1} ds \tag{20}$$

With $a = -6$ and $b = 0.45$, where the parameter λ is given by,

$$\lambda = \frac{\theta_1^2}{\nu}\frac{\partial u_e}{\partial s} \tag{21}$$

Laminar to Turbulent transition The laminar set of equations is closed with the amplification envelope slope correlation, which using the Falkner-Skan velocity profile family solves the Orr-Sommerfeld equation for the spatial amplification ratios of a series of shape parameters, unstable frequencies and Reynolds number, [16]. In order to determine the total amplification, n, at a streamwise position, s, starting from the stagnation point and moving downstream, the envelope slope has to be integrated as follows,

$$n(s) = \int_{Re_{\theta_1}^{CR}}^{Re_{\theta_1}} \frac{\partial n}{\partial Re_{\theta_1}} dRe_{\theta_1} \tag{22}$$

$$n_C = -8.43 - 2.4\, ln\,(TI) \tag{23}$$

Transition occurs when $n(s)$ reaches the critical amplification factor n_C, which directly depends on the turbulence intensity, TI, Equation (23).

3. Results

3.1. Two-dimensional steady computations

This section presents a detailed comparison of lift and drag coefficients as function of angle of attack between measurements, the 2D Navier-Stokes flow solver EllipSys2D, Xfoil and Q^3UIC. EllipSys2D computations used for benchmarking in the present report where published by Bertagnolio et al. in the Risø airfoil catalogue [18].

To check the ability of the codes to compute wind turbine airfoils, Figure 1 compares computations of flows past an FFA W3-241 airfoil [19] with experiments. From the figure Q^3UIC is seen to perform very well with respect to lift while the drag is slightly underpredicted at low and medium range of angles of attack.

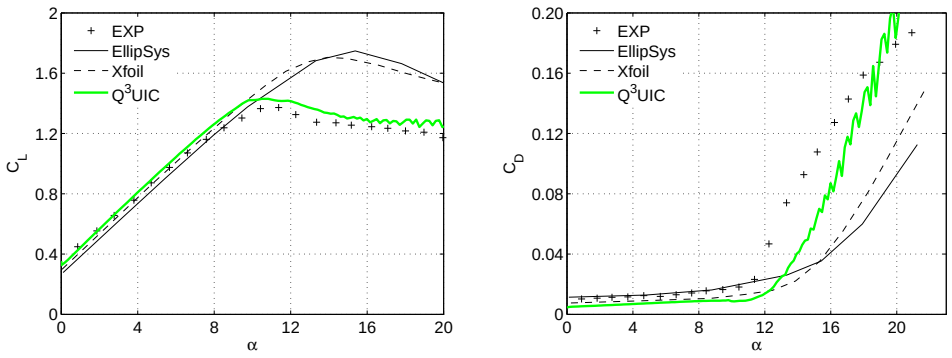

Figure 1. Lift and drag coefficient as a function of angle of attack for a FFA W3-241 at $Re = 1.5 \cdot 10^6$.

Another wind turbine airfoil used for validating the code is the S814 airfoil. The results from the computations for this airfoil geometry are shown in Figure 2. As in previous simulations a better stall behavior is obtained with the present model, exhibiting in overall similarly good results.

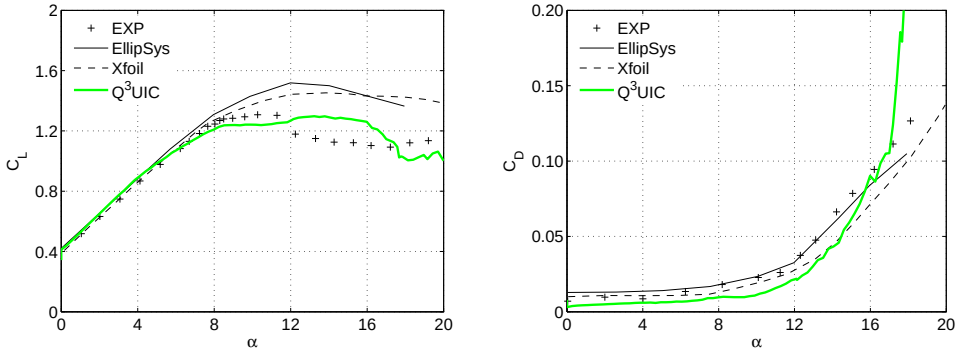

Figure 2. Lift and drag coefficient as a function of angle of attack for a S814 at $Re = 1.0 \cdot 10^6$.

Finally, in order to verify the ability of the code to compute thick airfoils, computations were carried out for the 30% thick FFA W3-301 airfoil [19]. The results from these computations

are shown in Figure 3. It is here seen that all computing codes have problems in determining the correct behavior in the stalled region. The new viscous-inviscid interactive code, however, seems to be capable of predicting the correct maximum lift value. It should be noted that as the thickness of airfoil increases the sensitivity to turbulence intensity also increases. A higher turbulent intensity will trigger the laminar to turbulent transition earlier, consequently the trailing edge separation will appear at lower angles of attack, moving upstream, and hence a lower maximum lift value will be predicted.

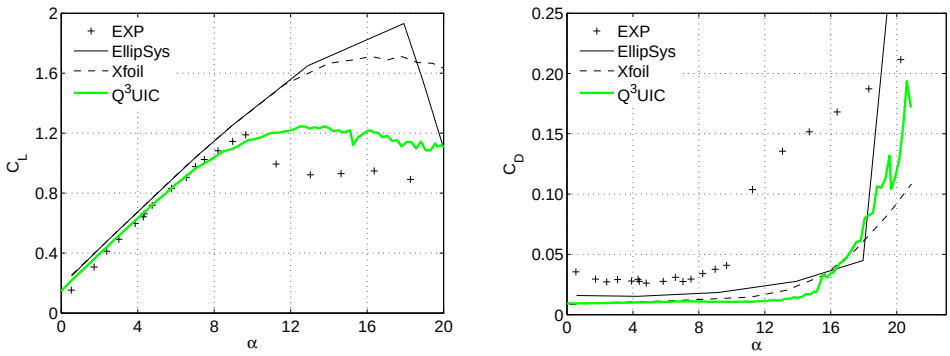

Figure 3. Lift and drag coefficient as a function of angle of attack for a FFA W3-301 at $Re = 1.5 \cdot 10^6$

3.2. Two-dimensional unsteady computations

Dynamic stall conditions are common on wind turbine rotors and affect their aerodynamic performance. Dynamic stall on a wind turbine blade can be induced by rotor yaw, blade control dynamics, flow control devices or changes in inflow conditions due to the turbulent nature of the atmospheric boundary layer. Most of these unsteady variations in flow characteristics are seen from the blade as a temporal change of angle of attack. Hence accurate predictions of the blade dynamic loads are of great importance in order to design new wind turbines blades with lower cost and better performance.

To validate the ability of the unsteady version of Q^3UIC to simulate dynamic stall the NACA 0015 airfoil was chosen. Experiments reported by Galbraith et al. [17] performed at the University of Glasgow are used for the code validation. Computed values of C_N and C_T are compared against measurements in Figure 4.

3.3. Two-dimensional inviscid double-wake computations

Because of poor performance of the single wake model in deep stall conditions, a new approach for computing airfoil performance at high angles of attack has been developed. Knowing that the low performance is due to the lack of accuracy of solving the integral boundary layer equations for flows with massive separation, in the new model the boundary layer is neglected and the flow is considered purely inviscid. Instead the pressure in the separated region is modeled by introducing an extended inviscid panel method. This model is referred to as the double wake model, due to the dual treatment of the separated region in two shear layers leaving the airfoil and converging downstream.

The bubble type of separation has been studied widely and the difficulties of modeling this kind of phenomena stems from the problem of predicting the pressure level in the separated region as well as determining the exact position where the attached boundary layer undergoes separation. The double wake model will generate a vortex sheet that leaves the airfoil from

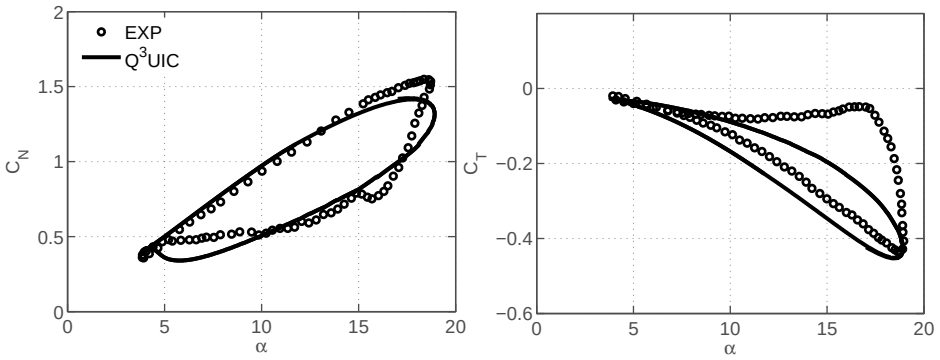

Figure 4. Comparison between computed and measured dynamic force coefficients of a NACA 0015 airfoil with: $\alpha_m = 11.37°$, $A = 7.55°$ and $k_A = 0.102$, and Re $= 1.5 \cdot 10^6$.

the separation point at the same time as the trailing edge is releasing vorticity through another vortex sheet. The uniform vortex distribution around the two wakes will influence the tangential velocities at the airfoil surface, creating a region of reversed flow, which simulates the separation effect of the flow around an airfoil at high angles of attack.

To validate the double wake model, the pressure distribution around the airfoil surface has been computed for the NACA 4412 airfoil in stalled conditions and compared against experiments, Figure 5. The separation position at which the upper wake is shed is guessed in this case from the experimental pressure distribution.

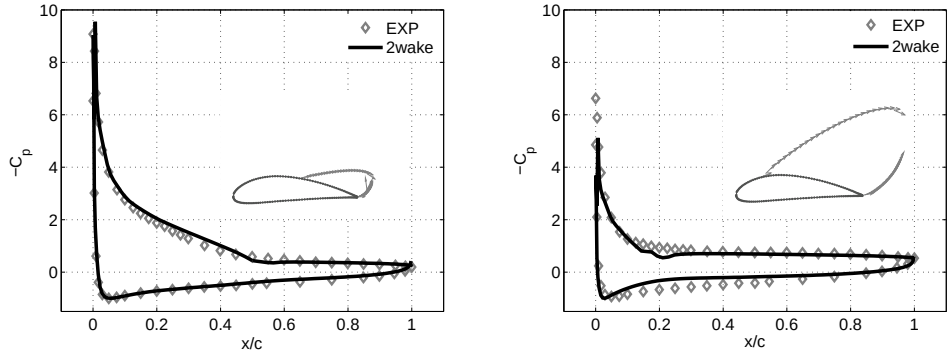

(a) (b)

Figure 5. Surface pressure coefficients of a NACA 4412 airfoil at Re $= 6.3 \cdot 10^6$ (a) $\alpha = 17.6°$; (b) $\alpha = 22.1°$

For extensive regions of separated flows, the separation point is guessed to appear in the leading edge region at the panel tangent to the freestream flow. Figure 6 shows a comparison of the C_L and C_D values predicted by the model and experiments. At low angles of attack the single wake VII model (Q^3UIC) is used while in the deep stall region simulations are performed using the double wake model.

3.4. Study of rotational effects

A parametric study on rotational effects in the boundary layer has been done on a NACA63418 airfoil using Q^3UIC. It shows that the effects of rotation are to decrease the growth of the

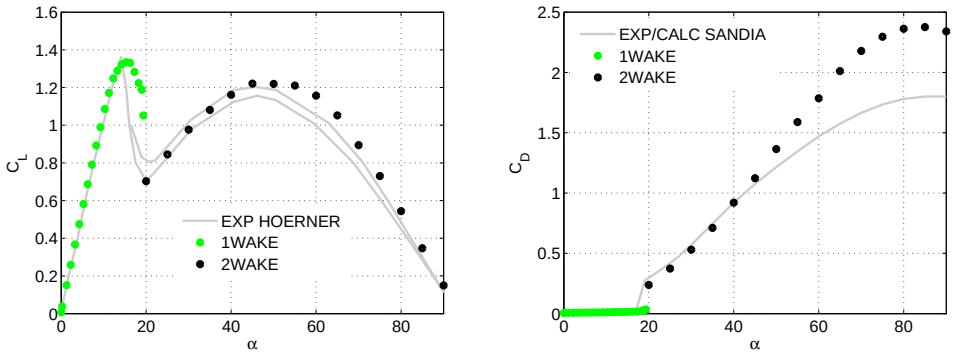

Figure 6. C_L and C_D as a function of α for a NACA 0012 airfoil. Single viscous and double wake inviscid computations.

boundary layer and delay the onset of separation as seen from the values of the friction coefficient, C_f, and the streamwise displacement thickness, δ_1^*, presented in Figure 8. From the figures it can be discerned how these effects gradually increase as the airfoil approaches the blade root, larger c/r ratio, increasing the lift coefficient at the same time as the drag is reduced at high angles of attack, see Figure 7. It must be noted how just before stall takes place, the growth of C_f due to rotation induces a special behavior in the C_D curve, increasing due to the higher friction drag and dropping as soon as the flow separates.

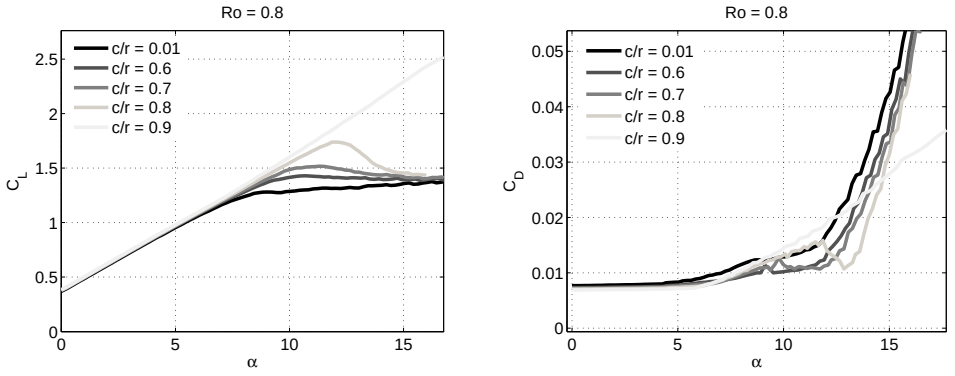

Figure 7. C_L and C_D of a NACA 63418 airfoil as a function of α at different values of c/r and $Ro = 0.8$ at $Re = 1.0 \cdot 10^6$.

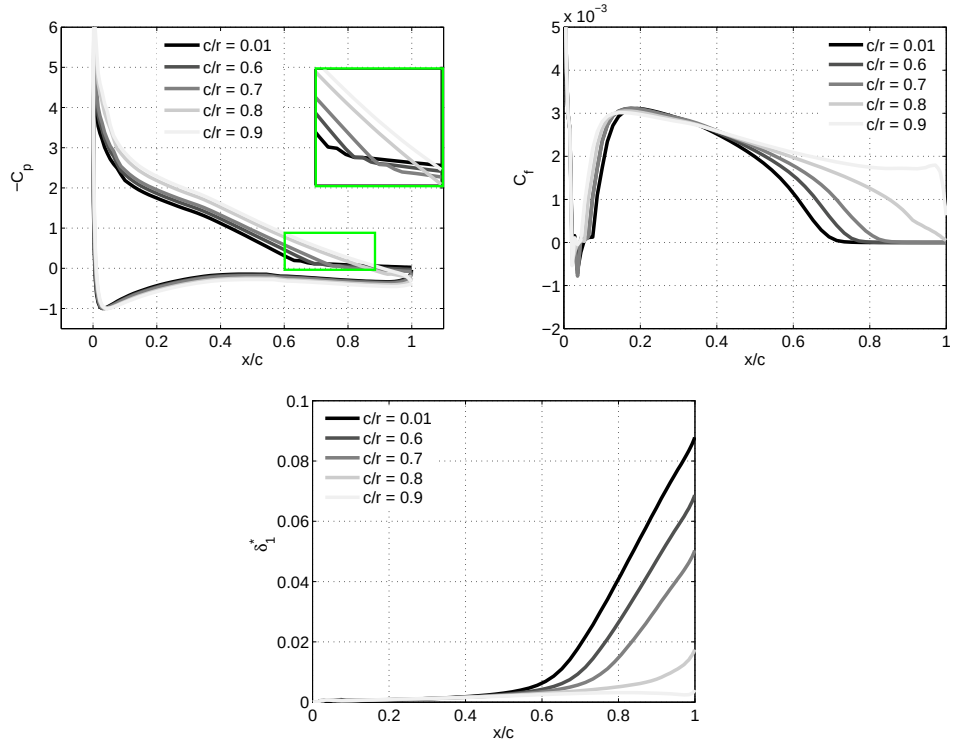

Figure 8. C_p, C_f and δ_1^* at $\alpha = 12^\circ$ on the upper side of a NACA 63418 airfoil at different values of c/r and $Ro = 0.8$ at $Re = 1.0 \cdot 10^6$.

4. Conclusion and future work

The Q^3UIC computing code presented herein has been developed during the last four years to become a design tool for wind turbine airfoils. It is capable of computing aerodynamic performance of airfoils under rotation and unsteady effects with high accuracy and low computational costs. A study of airfoil aerodynamic performance in steady and unsteady conditions has been presented for validation of the Q^3UIC code against experiments and other existing codes. An excellent agreement is obtained against experiments for the predicted aerodynamic lift, while drag is slightly under predicted. A study on the influence of rotation showed that Coriolis and centrifugal forces act as a favorable streamwise pressure gradient that thinners the boundary layer, reducing the airfoil obstruction against the freestream, moving the separation point downstream, and therefore increasing the lift. The drag coefficient is slightly increased by rotation in the original stall region and reduced after stall takes place.

In the near future the present code will be used to correct with viscous effects a full three-dimensional panel method running with a free vortex wake. The values of streamwise and spanwise boundary layer thickness computed with the quasi-3D method will be used to simulate a three dimensional transpiration velocity that will include the influence of a rotating boundary layer into the three dimensional potential flow solution.

Acknowledgments

We gratefully acknowledge the support from the Danish Council for Strategic Research for the project 'Center for Computational Wind Turbine Aerodynamics and Atmospheric Turbulence' (2104-09-067216/DSF), the Danish National Advanced Technology Foundation for the project 'Development of Adaptative Trailing Edge Flaps for Wind Turbines' (028-2007-3) and the Danish Energy Agency (EUDP) for the project 'Aeroelastic Optimization of MW Wind Turbines'.

References

[1] García N R 2011 Unsteady viscous-inviscid interaction technique for wind turbine airfoils *PhD. Thesis, Danmarks Tekniske Universitet*
[2] Le Balleur J C 1981 Strong matching method for computing transonic viscous flows including wakes and separations *La Recherche Aérospatiale* **3** 21
[3] Cebeci T and Jang H M 1990 Interactive boundary-layer method for unsteady airfoil flows: quasisteady model *Journal of Aircraft* **27** 673
[4] Drela M and Giles M B 1987 Viscous-inviscid analysis of transonic and low Reynolds number airfoils *AIAA journal* **25** 1347
[5] Sørensen J N 1988 Prediction of separated fLow past airfoils using viscous-inviscid interaction technique *La Recherche Aérospatiale* **3** 1
[6] Hess J L 1971 Numerical solution of inviscid subsonic flows *Von Karman Institute for Fluid Dynamics, Lecture Series* **34**
[7] Lighthill M J 1958 On displacement thickness *Journal of Fluid Mechanics*
[8] Mack L M 1977 Transition and laminar instability *National Aeronautics and Space Administration, Jet Propulsion Laboratory* **77-15**
[9] Katz J and Plotkin A 1977 Low speed aerodynamics: from wing theory to panel methods *McGraw-Hill*
[10] Cooke J C and Hall M G 1962 Boundary layers in three dimensions *Progress in Aero. Sci.* **2**
[11] Fogarty L E and Sears W R 1950 Potential flow around a rotating, advancing cylindrical blade *Journal of Aero. Sci.*. **17**
[12] Lakshminarayana B and Govindan T R 1981 Analysis of turbulent boundary layer on cascade and rotor blades of turbomachinery *AIAA journal.* **19** 1333
[13] Du Z and Selig M S 2000 The effect of rotation on the boundary layer of a wind turbine blade *Renewable Energy*
[14] Vasilis A R and Spyros G V 2008 Dynamic stall modeling on airfoils based on strong viscous-inviscid interaction coupling *International journal for numerical methods in fluids.* **56** 185
[15] Thwaites B 1949 Approximate calculation of the laminar boundary layer *The aeronautical Quarterly* **1** 245
[16] Gleyzes C, Cousteix Jr. and Bonnet J L 1950 Theoretical an experimental study of low Reynolds number transitional separation bubbles *Conference of Low Reynolds number Airfoil Aerodynamics, University of Notre Dame* **17**
[17] Galbraith R A M, Gracey M W and Leich E 1992 Summary of pressure data for thirteen aerofoils on the University of Glasgow's aerofoil database *G.U Aero report 9221, University of Glasgow*
[18] Bertagnolio F, Sørensen N and Johansen J 2001 Wind turbine airfoil catalogue *Risø-R-1280(EN)*
[19] Björck A 1990 Coordinates and calculations for the FFA-W1-xxx, FFA-W2-xxx and FFA-W3-xxx series of airfoils for horizontal axis wind turbines *FFA TN 1990-15, Flygtekniska Försöksanstalten*